

# Evolutionary Population Synthesis for Binary Stellar Population at High Spectral Resolution: Integrated Spectral Energy Distributions and Absorption-feature Indices

Fenghui Zhang,<sup>\*</sup> Lifang Li and Zhanwen Han

*National Astronomical Observatories/Yunnan Observatory, Chinese Academy of Sciences, PO Box 110, Kunming, Yunnan Province, 650011, China*

6 November 2018

## ABSTRACT

Using evolutionary population synthesis we present high resolution ( $0.3 \text{ \AA}$ ) integrated spectral energy distributions from 3000 to 7000  $\text{\AA}$  and absorption-line indices defined by the Lick Observatory image dissector scanner (referred to as the Lick/IDS) system, for an extensive set of instantaneous burst binary stellar populations with binary interactions. The ages of the populations are in the range 1 – 15 Gyr and the metallicities are in the range 0.004 – 0.03. This high resolution synthesis results can satisfy the needs of modern spectroscopic galaxy surveys, and are available on request.

By comparing the synthetic continuum of populations at high and low resolution we show that there is a good agreement for solar metallicity and a tolerable disagreement for non-solar metallicity. The strength of the Balmer lines at high spectral resolution is greater than that at low resolution for all metallicities. The comparison of Lick/IDS absorption-line indices at low and high resolution, both of which are obtained by the fitting functions, shows that the discrepancies in all indices except for  $\text{TiO}_1$  and  $\text{TiO}_2$  are insignificant for populations with  $Z = 0.004$  and  $Z = 0.02$ . The high resolution  $\text{Ca}4227$ ,  $\text{Fe}5015$  and  $\text{Mg}_b$  indices are redder than the corresponding low resolution one for populations with  $Z = 0.01$  and  $Z = 0.03$ , this effect lowers the derived age and metallicity of the population. The high resolution  $\text{Mg}_1$ ,  $\text{Fe}5709$  and  $\text{Fe}5782$  indices are bluer than those at low resolution, it raises the age and metallicity. The discrepancy in these six indices is greater for populations with  $Z = 0.03$  in comparison to  $Z = 0.01$ .

At high resolution we compare the Lick/IDS spectral absorption indices obtained by using the fitting functions with those measured directly from the synthetic spectra, and see that  $\text{Ca}4455$ ,  $\text{Fe}4668$ ,  $\text{Mg}_b$  and  $\text{Na D}$  indices obtained by the use of the fitting functions are redder for all metallicities,  $\text{Fe}5709$  is redder at  $Z = 0.03$  and becomes to be bluer at  $Z = 0.01$  and  $0.004$ , and other indices are bluer for all metallicities than the corresponding values measured directly from the synthetic spectra.

**Key words:** Star: evolution – binary: general – Galaxies: cluster: general

## 1 INTRODUCTION

In the previous papers (Zhang et al. 2004, 2005, hereinafter Paper I, II), we took into account various known classes of binary stars in evolutionary population synthesis (EPS) models, presented integrated colours, integrated spectral energy distributions (ISEDs) and 21 absorption-line indices

[following the definitions of Worthey et al. 1994] defined by the Lick Observatory image dissector scanner (referred to as the Lick/IDS) system for an extensive set of instantaneous-burst binary stellar populations (BSPs) with binary interactions, investigated the influences of binary interactions and model input parameters on the results, and found that the inclusion of binary interactions makes the integrated  $U - B$ ,  $B - V$ ,  $V - R$  and  $R - I$  colours and the 21 Lick/IDS spectral indices substantially bluer. In Papers I and II the

<sup>\*</sup> E-mail: gssephd@public.km.yn.cn; zhang\_fh@hotmail.com

corrected BaSeL-2.0 (i.e., non-calibrated BaSeL-2.2) stellar spectra library of Lejeune, Cuisinier & Buser (1997, 1998) was used and low spectral resolution ISEDs (10 Å in the ultraviolet and 20 Å in the visible) were given.

In recent years, some spectroscopic galaxy surveys at intermediate spectral resolution (such as the Sloan Digital Sky Survey, SDSS) have been undertaken, and the data has been analyzed with EPS models to understand galaxy formation and evolution. Therefore, a EPS model that can predict the ISEDs at intermediate and high spectral resolution is required. The high spectral resolution of ISEDs can be used to predict the strength of numerous weak absorption lines and the evolution of the profiles of the strongest lines over a wide range of ages (González Delgado et al. 2005). And, the higher the spectral resolution, the higher the constraining power (Vazdekis 1999). Therefore, in this paper we attempt to include high resolution spectral information in our EPS models.

So far, the majority of EPS studies used low resolution stellar spectral library as an ingredient. In the EPS models of Vazdekis (1999) and Bruzual & Charlot (2003) intermediate spectral resolution ISEDs were provided: the former used a subsample of  $\sim 500$  stars from the original Jones (1997) empirical stellar library and presented the ISEDs of single stellar populations (SSPs) with a spectral resolution of  $\sim 1.8$  Å in two reduced spectral regions: 3856 – 4476 and 4795 – 5465 Å, the latter used the STELIB library (Le Borgne et al. 2003) and presented 3 Å resolution models covering 3200 – 9500 Å with their code GALAXEV. In addition, EPS models also can use the intermediate-resolution empirical stellar library of Sánchez-Blazquez et al. (2003), which comprises  $\sim 1100$  stars and covers the spectral range 3500 – 7500 Å with a resolution of  $\sim 2$  Å.

With the emergence of new-generation empirical (e.g., the ELODIE data base of Prugniel & Soubiran 2001) and theoretical (Bertone et al. 2003a; Castelli & Munari 2001; Chavez, Malagnini & Morossi 1997; González Delgado & Leitherer 1999; González Delgado et al. 2005; Munari et al. 2005; Murphy & Meiksin 2004; Zwitter, Castelli & Munari 2002, 2004) stellar spectral libraries, EPS models can present the high-resolution ISEDs and spectral absorption indices. Bertone et al. (2003b) used their library and explored the spectral properties of SSPs in the optical (4880–5390 Å) and ultraviolet regions (2275–2575 Å and 2690–2960 Å) at  $R = 500\,000$  and  $50\,000$ , respectively. Tantalo et al. (2004) used the library of Munari et al. (2005) and presented the Lick absorption-line indices of SSPs from their 1-Å resolution spectra. Recently, González Delgado et al. (2005) used their library and presented high resolution theoretical spectra ( $\sim 0.3$  Å) of SSPs in the 3000 – 7000 Å range.

In the few EPS studies to date that have presented intermediate and high spectral resolution results, binary interactions are neglected. Binary stars play an important role in determining the overall appearance of any realistic stellar population (Xin & Deng 2005, and Papers I and II for an extensive discussion), therefore, in this paper we intend to use the high resolution stellar spectral library in our EPS study of BSPs and present their ISEDs and Lick/IDS absorption-feature indices. This set of indices includes 21 indices of Worthey et al. (1994) and 4 Balmer indices defined

by Worthey & Ottaviani (1997). In an instantaneous burst BSP all stars are assumed to be born in binaries and born at the same time, and  $1 \times 10^6$  binary systems are comprised.

The outline of the paper is as follows: we describe our EPS models and algorithm in Section 2; our results are presented in Section 3, and then finally, in Section 4, we give our conclusions.

## 2 MODEL DESCRIPTION

### 2.1 Initialization of the binary population

We first need to construct the instantaneous burst BSPs. A Monte Carlo process is used to produce a population of  $1 \times 10^6$  binary systems, and the initial state of each binary satisfies the following input distributions:

(i) the initial mass function (IMF) of the primaries, which gives the relative number of the primaries in the mass range  $m_1 \rightarrow m_1 + dm_1$ . In this study the initial mass of the primary is chosen from the approximation to the IMF of Miller & Scalo (1979) as given by Eggleton, Fitchett & Tout (1989, hereinafter EFT),

$$m_1 = \frac{0.19X}{(1-X)^{0.75} + 0.032(1-X)^{0.25}}, \quad (1)$$

where  $X$  is a random variable uniformly distributed in the range  $[0,1]$ , and  $m_1$  is the primary mass in units of  $M_\odot$ .

(ii) the initial secondary-mass distribution, which is assumed to be correlated with the initial primary-mass distribution in this study. So, it depends on the initial primary-mass (as set by equation 1) and the initial mass ratio,  $q$ , distribution, which is assumed to be a uniform form (EFT 1989; Mazeh et al. 1992; Goldberg & Mazeh 1994),

$$n(q) = 1, \quad 0 \leq q \leq 1, \quad (2)$$

where  $q = m_2/m_1$ ,  $m_2$  is the secondary mass in units of  $M_\odot$ .

(iii) the distribution of orbital separations (or periods). It is taken as constant in  $\log a$  (where  $a$  is the separation) for wide binaries and falls off smoothly at close separations:

$$a n(a) = \begin{cases} a_{\text{sep}}(a/a_0)^\psi, & a \leq a_0, \\ a_{\text{sep}}, & a_0 < a < a_1, \end{cases} \quad (3)$$

where  $a_{\text{sep}} \approx 0.070$ ,  $a_0 = 10 R_\odot$ ,  $a_1 = 5.75 \times 10^6 R_\odot$  and  $\psi \approx 1.2$ .

(iv) the eccentricity distribution. A uniform form is assumed:

$$e = X, \quad (4)$$

where  $X$  is a random variable, as in Eq. (1).

After the initial state (the masses of the component stars,  $m_1$  and  $m_2$ , the separation  $a$  and eccentricity  $e$  of the orbit) of a binary system in a BSP is set, we also need to set the lower and upper mass cut-offs  $m_l$  and  $m_u$  to the mass distributions and assign a metallicity  $Z$  to the stars:  $m_l$  and  $m_u$  are set as 0.1 and  $100 M_\odot$ , respectively,  $Z = 0.004, 0.01, 0.02, 0.03$ . The relative age  $\tau$  of the BSP is assigned within the range of 1 – 15 Gyr.

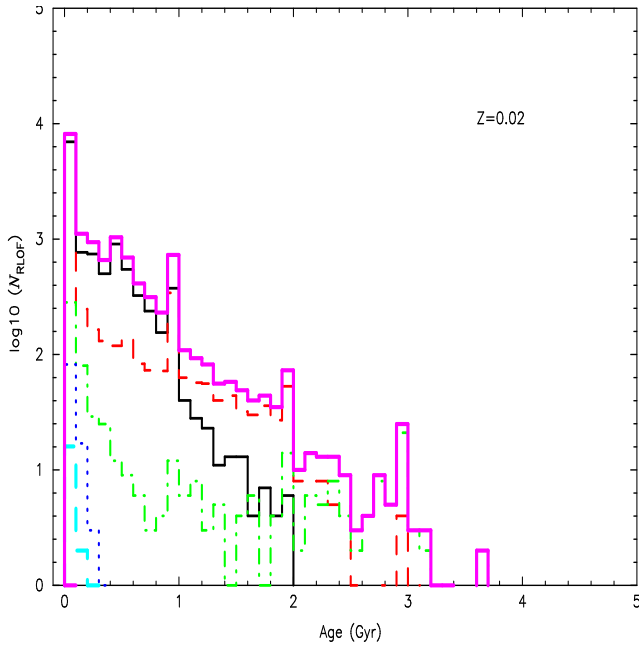


**Figure 1.** Number of binary systems experiencing RLOF as a function of time for solar-metallicity BSPs of  $1 \times 10^6$  binaries. Solid, dashed, dot-dashed, dotted, thick-dashed and thick-solid lines represent the 1st, 2nd, 3rd, 4th, 5th and all RLOF, respectively.

## 2.2 Input physics, parameters and algorithm

We use the rapid binary star evolution (BSE) algorithm of Hurley, Tout & Pols (2002) to evolve each binary in the BSP to an age of  $\tau$ , which gives us evolutionary parameters such as the stellar luminosity  $L$ , effective temperature  $T_{\text{eff}}$ , radius  $R$ , current mass  $m$  and the ratio of radius to Roche-lobe radius  $R/R_L$  for the component stars. Next we use the high resolution HRES stellar spectral library of González Delgado et al. (2005) to transform the evolutionary parameters to stellar flux by interpolating the flux grid in the  $\log T_{\text{eff}} - \log g - [\text{Fe}/\text{H}]$  plane, and then use equation (5) to obtain the monochromatic flux for an instantaneous BSP of a particular age and metallicity. For the spectral absorption-line indices in the Lick/IDS system, we obtain them by two methods: (i) measure them directly from the synthetic flux, (ii) use the empirical fitting functions of Worthey et al. (1994) and Worthey & Ottaviani (1997) to assign the Lick/IDS absorption indices to a star with a set of given evolutionary parameters, and then use equations (6)–(8) to derive the indices for a BSP.

The integrated monochromatic flux of a BSP is defined as

$$F_{\lambda, \tau, Z} = \sum_{k=1}^n f_{\lambda}, \quad (5)$$

where  $f_{\lambda}$  is the SED of the  $k$ th star.

The integrated absorption feature index of the Lick/IDS system is a flux-weighted one. For the  $i$ th atomic absorption line, it is expressed in equivalent width ( $W$ , in angstroms),

$$W_{i, \tau, Z} = \frac{\sum_{k=1}^n w_i \cdot f_{i, C\lambda}}{\sum_{k=1}^n f_{i, C\lambda}}, \quad (6)$$

where  $w_i$  is the equivalent width of the  $i$ th index of the  $k$ th star, and  $f_{i, C\lambda}$  is the continuum flux at the midpoint of the  $i$ th ‘feature’ passband. The local continuum for the  $i$ -th index is the run of flux defined by drawing a straight line from the midpoint of the blue pseudocontinuum level to the midpoint of the red pseudocontinuum level, the flux at the midpoint of pseudocontinuum is an average one and obtained by

$$f_{i, p} = \frac{\int_{\lambda_{i,1}}^{\lambda_{i,2}} f_{\lambda} d\lambda}{\lambda_{i,2} - \lambda_{i,1}}, \quad (7)$$

where  $f_{\lambda}$  is the stellar flux, as in Eq. (5),  $\lambda_{i,1}$  and  $\lambda_{i,2}$  are the wavelength limits of the  $i$ -th pseudocontinuum sideband. For the  $i$ th molecular line, the feature index is expressed in magnitude,

$$C_{i, \tau, Z} = -2.5 \log \frac{\sum_{k=1}^n 10^{-0.4c_i} \cdot f_{i, C\lambda}}{\sum_{k=1}^n f_{i, C\lambda}}, \quad (8)$$

where  $c_i$  is the magnitude of the  $i$ th index of the  $k$ th star.

Detailed descriptions of the BSE package of Hurley et al. (2002) and the empirical fitting functions of Worthey et al. (1994) have been presented in Papers I and II, here we only mention several important input parameters required in the BSE code: the efficiency of common envelope ejection  $\alpha_{\text{CE}}$  is taken as 1.0, the Reimers wind mass-loss coefficient  $\eta$  is set constant at 0.3, and the tidal enhancement parameter  $B = 0.0$ .

Following, we present a brief description of the HRES stellar spectral library of González Delgado et al. (2005). A full discussion is given in Martins et al. (2005). This library includes the synthetic stellar spectra from 3000 to 7000 Å with a final spectral sampling of 0.3 Å. The spectra span a range of effective temperature from 3000 to 55000K, with variable steps from 500 to 2500K, and a surface gravity  $\log g = -0.5$  to 5.5 with dex steps of 0.25 and 0.5. For each temperature, the minimum gravity is set by the Eddington limit. The library covers several metallicities: twice solar, solar, half solar and 1/10 solar. Solar abundance ratios for all the elements, and a helium abundance of He/H = 0.1 by number are assumed. This high spectral resolution stellar library is based on Kurucz local thermodynamic equilibrium (LTE) atmospheres (Kurucz 1993) and the program SYNSPEC (Hubeny, Lanz & Jeffery 1995) for stars with  $8000 \leq T_{\text{eff}} \leq 27000$  K, the program SPECTRUM (Gray & Corbally 1994) and Kurucz atmospheres for stars with  $4750 \leq T_{\text{eff}} \leq 7750$  K, non-LTE line-blanketed models for hot ( $27500 \leq T_{\text{eff}} \leq 55000$  K, Lanz & Hubeny 2003), and PHOENIX LTE line-blanketed models for cool stars ( $3000 \leq T_{\text{eff}} \leq 4500$  K, Hauschildt & Baron 1999; Allard et al. 2001). This library is composed of 1650 spectra.

By adopting the above set of input distributions and parameters, in Fig. 1 we present the number of binary systems experiencing Roche lobe overflow (RLOF) as a function of time for solar-metallicity BSPs of  $1 \times 10^6$  binaries. Because some binary systems would experience RLOF for several times, in Fig. 1 solid, dashed, dot-dashed, dotted and thick-dashed and thick-solid lines represent the 1st, 2nd, 3rd, 4th, 5th and all RLOF, respectively. From Fig. 1 we see that RLOF mainly happens at early age, and the number decreases with time. During the past 15 Gyr  $\sim 11.6$  per cent of the binaries would experience RLOF.

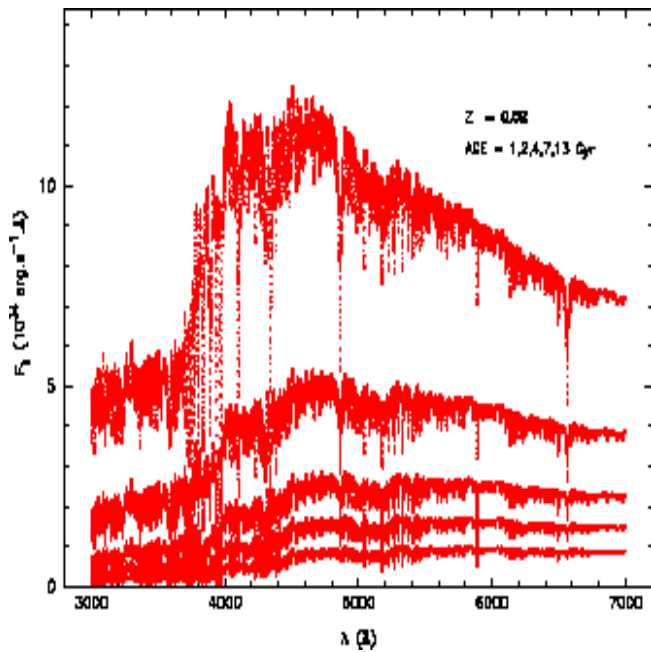


**Figure 2.** The high spectral resolution integrated spectral energy distributions as a function of age for solar-metallicity BSPs. From top to bottom, the ages  $\tau = 1, 2, 4, 7, 13$  Gyr, respectively.

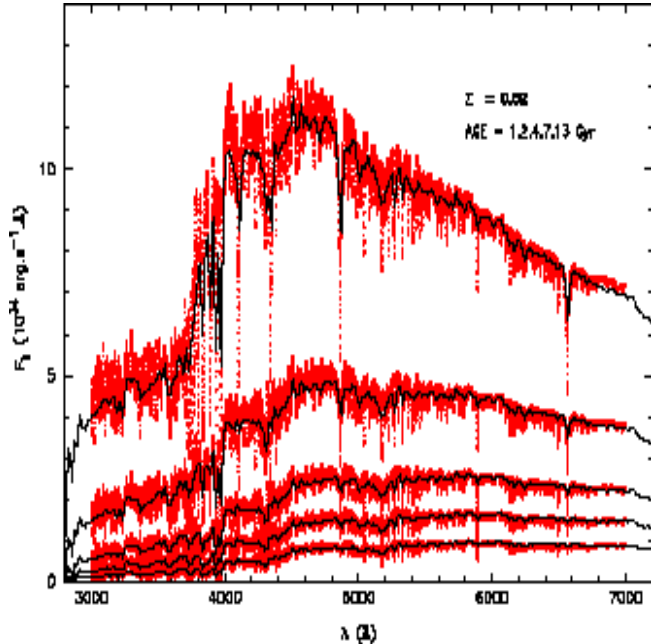


**Figure 4.** Comparison of the high resolution (solid line) with low resolution (dots) integrated spectral energy distributions for solar-metallicity BSPs at ages  $\tau = 1, 2, 4, 7$  and  $13$  Gyr (from top to bottom, respectively).

### 3 RESULTS

#### 3.1 The integrated spectral energy distribution

In this part we present ISEDs covering the range  $3000 - 7000 \text{ \AA}$  with a resolution of  $0.3 \text{ \AA}$  for instantaneous burst BSPs with binary interactions over a large range of age and metallicity:  $1 \leq \tau \leq 15$  Gyr and  $-1.3 \leq [\text{Fe}/\text{H}] \leq +0.2$ . For

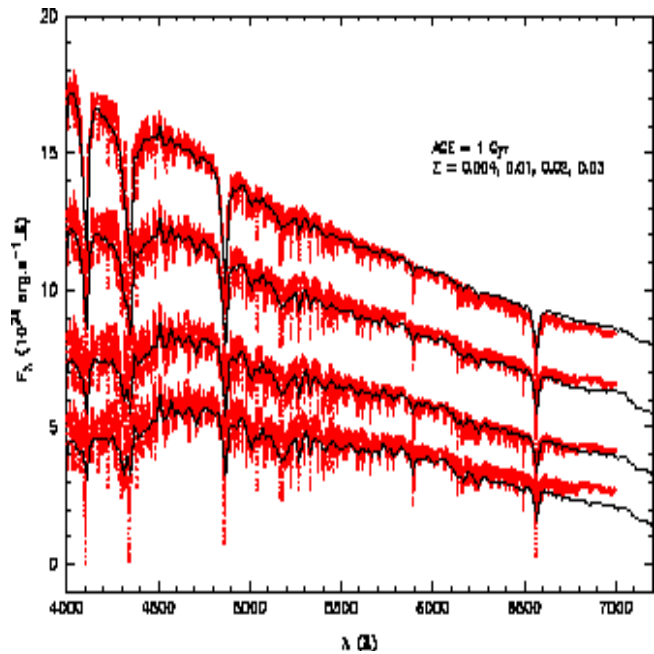


**Figure 5.** Comparison between the high (solid line) and low resolution (dots) integrated spectral energy distributions for  $\tau = 1$  Gyr BSPs with  $Z = 0.004, 0.01, 0.02$  and  $0.03$  (from top to bottom, respectively). For the sake of clarity the fluxes at metallicities of  $0.01, 0.02$  and  $0.03$  are shifted downwards by an amount of  $1.5$ .

each model, a total of  $1.0 \times 10^6$  binaries are evolved according to the algorithm given in the previous section. The full set ISEDs are available on request from the authors.

In Fig. 2 we give the high spectral resolution ISED evolution for solar-metallicity BSPs at ages  $\tau = 1, 2, 4, 7$  and  $13$  Gyr in the wavelength range of  $3000 - 7000 \text{ \AA}$ . It shows that the continuum tends to be redder with increasing the age of the BSP, the variation in the shape of the continuum with time is significant at early age, and is almost constant at intermediate and late ages. Additionally, Fig. 2 shows that the strength of the Balmer lines decreases with the age of the BSP.

The metallicity effect on ISED evolution of BSPs is shown in the top panel of Fig. 3, which presents the ISEDs of young ( $\tau = 1$  Gyr) and intermediate-age ( $\tau = 7$  Gyr) BSPs at four different metallicities:  $Z = 0.004, 0.01, 0.02, 0.03$ . The metallicity effect is also exhibited in the slope of the continuum and in the strength of the metallic lines. The continuum tends to be redder with increasing metallicity and metallic lines to be stronger. The bottom panel of Fig. 3 gives the evolution of Balmer lines with metallicity, it shows that their strength tends to be weaker when increasing metallicity.

In Fig. 4 we compare the ISEDs at high and low spectral resolution ( $10 \text{ \AA}$  in the ultraviolet and  $20 \text{ \AA}$  in the visible) for solar-metallicity BSPs at ages  $\tau = 1, 2, 4, 7$  and  $13$  Gyr. These low resolution ISEDs are from Model A of Paper II, which includes binary interactions and adopts the same input parameters and distributions as this paper except for using the corrected BaSeL-2.0 (i.e., non-calibrated BaSeL-2.2) stellar spectral library of Lejeune et al. (1997, 1998). Fig. 4 shows that there is a good agreement in the continuum for solar-metallicity BSPs between two studies. Comparison

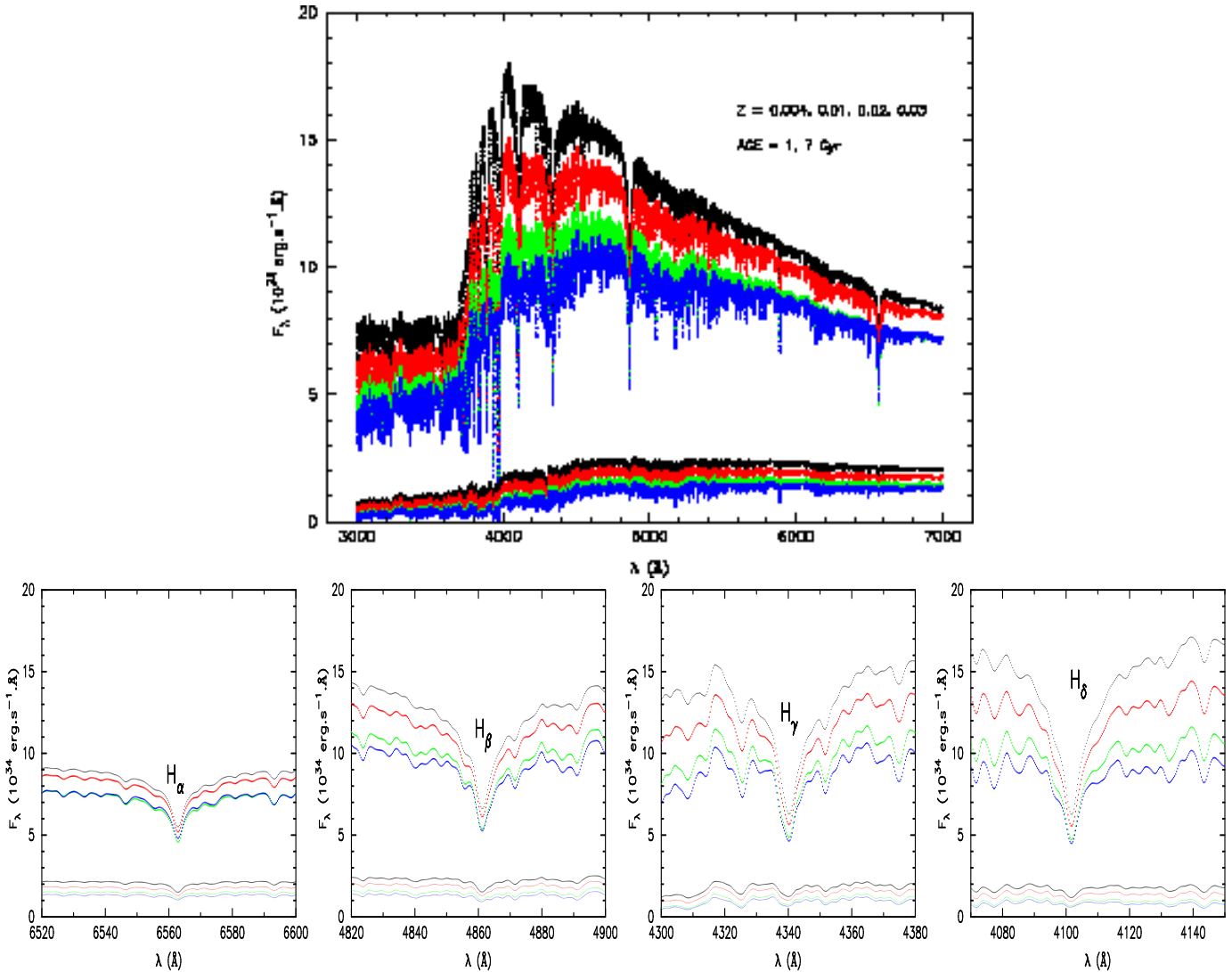


**Figure 3.** The high resolution integrated spectral energy distributions (top panel) and Balmer lines (bottom panel) as a function of metallicity (From top to bottom, the metallicity  $Z = 0.004, 0.01, 0.02$  and  $0.03$ , respectively) for BSPs at ages  $\tau = 1$  and  $7$  Gyr.

of the continuum for BSPs with non-solar metallicity shows that there is a difference existed at longer wavelengths for BSPs at ages  $\tau = 1$  and  $2$  Gyr. In Fig 5 we give the ISEDs at high and low resolution for  $\tau = 1$  Gyr BSP with four metallicities. It shows that at longer wavelengths the high resolution continuum is lower (redder) for BSPs with  $Z = 0.004$ , while greater (bluer) for BSPs with  $Z = 0.01$  and  $0.03$  than that at low resolution.

### 3.2 Lick spectral absorption feature indices

At high spectral resolution we use two methods to obtain 25 Lick/IDS spectral absorption indices defined by Worthey et al. (1994) and Worthey & Ottaviani (1997): (1) directly compute them from the high-resolution synthetic spectra, (2) obtain them by using the empirical fitting functions of Worthey et al. (1994) and Worthey & Ottaviani (1997).

All the following results are for BSPs of  $10^6$  binaries. To verify that our results are stable for  $10^6$  binaries, we

perform several simulations, the number of binaries in each simulation is  $10^4, 4 \times 10^4, 1.6 \times 10^5, 3.6 \times 10^5$  and  $6.4 \times 10^5$ , respectively. As an example, in Fig. 6 we plot the evolution of  $Mg_1$  index as a function of the number of binaries in the simulation, we see that the  $Mg_1$  index fluctuates around the value for  $10^6$  binaries when the number of binaries is not so enough, with the increase of the number of binaries the fluctuation would decrease. For  $10^4$  binaries the discrepancy reaches to  $\sim 0.05 \text{ \AA}$  at  $\tau = 12$  Gyr, for  $3.6 \times 10^5$  binaries  $Mg_1$  agrees with the value for  $10^6$  binaries within a small range, and for  $6.4 \times 10^5$  binaries the discrepancy is insignificant. Therefore the results for  $10^6$  binaries in the simulation are stable.

#### 3.2.1 Results by the use of the fitting functions

Using the high resolution spectra and the fitting functions of Worthey et al. (1994) and Worthey & Ottaviani (1997), we obtain 25 Lick/IDS spectral absorption indices for the BSPs with binary interactions with four metallicities from

**Table 1.** Lick/IDS spectral absorption feature indices of BSPs, derived by using the empirical fitting functions (Section 3.2.1).

	1.00	2.00	3.00	4.00	5.00	6.00	Age (Gyr)	8.00	9.00	10.00	11.00	12.00	13.00	14.00	15.00	
$Z = 0.004$																
CN <sub>1</sub>	-0.184	-0.136	-0.106	-0.079	-0.065	-0.051	-0.048	-0.048	-0.051	-0.038	-0.034	-0.032	-0.044	-0.038	-0.035	-0.036
CN <sub>2</sub>	-0.110	-0.077	-0.056	-0.037	-0.027	-0.015	-0.013	-0.015	-0.006	-0.003	-0.002	-0.002	-0.011	-0.006	-0.005	-0.006
Ca4227	0.157	0.334	0.436	0.523	0.589	0.657	0.699	0.683	0.709	0.744	0.777	0.770	0.774	0.830	0.830	0.802
G4300	-0.883	0.715	1.730	2.585	3.081	3.504	3.652	3.585	4.011	4.213	4.309	3.987	4.200	4.366	4.360	4.360
Fe4383	-0.377	0.419	1.131	1.703	2.026	2.341	2.433	2.501	2.691	2.824	2.887	2.848	3.021	3.130	3.169	3.169
Ca4455	0.213	0.480	0.639	0.757	0.845	0.919	0.961	0.951	0.982	1.015	1.049	1.041	1.055	1.085	1.085	1.067
Fe4531	1.041	1.556	1.830	2.054	2.187	2.320	2.369	2.340	2.422	2.481	2.521	2.493	2.547	2.580	2.562	2.562
Fe4668	-0.122	0.377	0.816	1.006	1.275	1.413	1.595	1.604	1.448	1.451	1.599	1.708	1.626	1.705	1.590	1.590
H $\beta$	5.564	4.352	3.585	2.984	2.690	2.415	2.360	2.394	2.159	2.054	2.018	2.179	2.030	1.956	1.950	1.950
Fe5015	2.028	2.872	3.299	3.412	3.700	3.796	4.025	4.039	3.793	3.832	3.998	4.137	3.897	3.989	3.820	3.820
Mg <sub>1</sub>	0.012	0.014	0.019	0.025	0.027	0.032	0.033	0.033	0.037	0.040	0.042	0.042	0.047	0.048	0.049	0.049
Mg <sub>2</sub>	0.062	0.078	0.092	0.100	0.109	0.116	0.121	0.122	0.122	0.127	0.133	0.138	0.144	0.144	0.142	0.142
Mg <sub>b</sub>	1.155	1.486	1.745	1.808	2.059	2.039	2.187	2.224	2.079	2.132	2.267	2.431	2.480	2.480	2.413	2.413
Fe5270	0.812	1.229	1.476	1.641	1.764	1.869	1.932	1.916	1.946	1.993	2.035	2.050	2.068	2.107	2.085	2.085
Fe5335	0.635	0.917	1.114	1.244	1.349	1.438	1.496	1.496	1.502	1.543	1.590	1.625	1.654	1.682	1.661	1.661
Fe5406	0.293	0.492	0.618	0.722	0.784	0.865	0.881	0.879	0.914	0.942	0.967	0.971	1.013	1.022	1.008	1.008
Fe5709	0.320	0.450	0.508	0.577	0.590	0.638	0.622	0.607	0.665	0.678	0.672	0.644	0.679	0.678	0.681	0.681
Fe5782	0.208	0.294	0.345	0.400	0.415	0.455	0.450	0.440	0.469	0.482	0.481	0.470	0.501	0.496	0.495	0.495
Na D	1.193	1.197	1.306	1.363	1.455	1.500	1.592	1.620	1.572	1.660	1.685	1.784	1.814	1.858	1.870	1.870
TiO <sub>1</sub>	0.033	0.033	0.035	0.030	0.034	0.032	0.039	0.040	0.029	0.030	0.034	0.041	0.033	0.034	0.030	0.030
TiO <sub>2</sub>	0.034	0.035	0.040	0.032	0.040	0.037	0.049	0.052	0.032	0.033	0.042	0.053	0.040	0.042	0.035	0.035
H $\delta$ A	8.599	6.626	4.769	3.260	2.467	1.824	1.574	1.517	0.959	0.678	0.536	1.062	0.679	0.347	0.349	0.349
H $\gamma$ A	7.834	4.965	2.626	0.815	-0.215	-1.137	-1.513	-1.587	-2.383	-2.748	-2.975	-2.340	-2.734	-3.164	-3.137	-3.137
H $\delta$ F	6.071	4.772	3.681	2.756	2.228	1.865	1.720	1.698	1.384	1.218	1.148	1.481	1.236	1.088	1.101	1.101
H $\gamma$ F	6.032	4.429	3.148	2.108	1.491	0.994	0.785	0.765	0.317	0.116	-0.012	0.321	0.112	-0.141	-0.128	-0.128
$Z = 0.01$																
CN <sub>1</sub>	-0.155	-0.088	-0.057	-0.046	-0.036	-0.022	-0.023	-0.013	-0.006	-0.002	-0.004	-0.004	-0.003	0.000	0.005	0.004
CN <sub>2</sub>	-0.092	-0.042	-0.018	-0.009	-0.001	0.012	0.012	0.021	0.027	0.026	0.028	0.029	0.031	0.034	0.034	0.034
Ca4227	0.309	0.563	0.689	0.754	0.767	0.892	0.856	0.931	0.904	0.963	1.010	1.033	1.037	1.037	1.050	1.055
G4300	0.134	2.241	3.195	3.526	3.806	4.208	4.156	4.441	4.657	4.694	4.794	4.809	4.902	5.114	5.072	5.072
Fe4383	0.421	1.820	2.592	2.910	3.318	3.565	3.625	3.851	4.026	4.088	4.137	4.203	4.304	4.407	4.421	4.421
Ca4455	0.497	0.862	1.024	1.105	1.155	1.253	1.237	1.306	1.356	1.363	1.382	1.402	1.421	1.439	1.453	1.453
Fe4531	1.526	2.166	2.443	2.560	2.660	2.798	2.782	2.898	2.972	2.987	3.000	3.028	3.066	3.089	3.111	3.111
Fe4668	0.837	2.010	2.460	2.752	2.830	3.178	3.081	3.246	3.381	3.360	3.421	3.477	3.480	3.468	3.485	3.485
H $\beta$	5.158	3.527	2.873	2.666	2.503	2.298	2.505	2.135	2.024	1.998	1.961	1.935	1.882	1.787	1.785	1.785
Fe5015	3.063	4.022	4.264	4.531	4.476	4.794	4.646	4.746	4.864	4.815	4.923	5.010	4.976	4.950	4.991	4.991
Mg <sub>1</sub>	0.012	0.024	0.035	0.039	0.046	0.051	0.052	0.059	0.062	0.064	0.064	0.066	0.069	0.070	0.073	0.073
Mg <sub>2</sub>	0.080	0.115	0.131	0.142	0.149	0.163	0.162	0.171	0.179	0.182	0.184	0.188	0.192	0.192	0.196	0.196
Mg <sub>b</sub>	1.505	2.137	2.263	2.482	2.479	2.752	2.679	2.770	2.893	2.920	3.021	3.101	3.010	3.102	3.113	3.113
Fe5270	1.305	1.846	2.071	2.185	2.258	2.380	2.371	2.459	2.521	2.536	2.558	2.587	2.610	2.625	2.635	2.635
Fe5335	1.015	1.496	1.702	1.805	1.878	1.993	1.978	2.068	2.128	2.144	2.155	2.186	2.209	2.213	2.243	2.243
Fe5406	0.513	0.837	1.007	1.070	1.145	1.218	1.224	1.297	1.341	1.346	1.348	1.371	1.392	1.394	1.416	1.416
Fe5709	0.476	0.613	0.704	0.720	0.768	0.779	0.798	0.828	0.839	0.841	0.834	0.838	0.852	0.857	0.865	0.865
Fe5782	0.323	0.463	0.539	0.560	0.599	0.621	0.628	0.660	0.674	0.662	0.669	0.681	0.681	0.675	0.684	0.684
Na D	1.323	1.677	1.834	1.948	2.006	2.145	2.144	2.219	2.295	2.351	2.380	2.417	2.441	2.465	2.501	2.501
TiO <sub>1</sub>	0.036	0.040	0.037	0.041	0.037	0.042	0.038	0.038	0.040	0.039	0.040	0.041	0.040	0.039	0.040	0.040
TiO <sub>2</sub>	0.037	0.047	0.044	0.051	0.045	0.057	0.047	0.049	0.053	0.051	0.053	0.056	0.054	0.051	0.053	0.053
H $\delta$ A	7.873	3.990	2.279	1.729	1.288	0.481	0.526	0.220	-0.448	-0.470	-0.687	-0.761	-0.876	-1.333	-1.229	-1.229
H $\gamma$ A	6.677	1.902	-0.309	-1.093	-1.710	-2.707	-2.638	-3.291	-3.859	-3.901	-4.149	-4.264	-4.375	-4.905	-4.806	-4.806
H $\delta$ F	5.447	3.210	2.226	1.925	1.690	1.275	1.342	1.074	0.830	0.833	0.728	0.691	0.634	0.412	0.464	0.464
H $\gamma$ F	5.315	2.758	1.541	1.104	0.781	0.236	0.274	-0.072	-0.372	-0.408	-0.557	-0.620	-0.676	-0.969	-0.913	-0.913
$Z = 0.02$																
CN <sub>1</sub>	-0.121	-0.060	-0.028	-0.009	0.006	0.018	0.030	0.023	0.035	0.048	0.050	0.045	0.058	0.032	0.065	0.065
CN <sub>2</sub>	-0.065	-0.018	0.009	0.026	0.040	0.050	0.062	0.057	0.068	0.080	0.083	0.077	0.091	0.070	0.097	0.097
Ca4227	0.428	0.714	0.878	0.964	1.045	1.085	1.187	1.155	1.206	1.310	1.329	1.251	1.356	1.256	1.434	1.434
G4300	1.045	2.947	3.784	4.210	4.583	4.873	5.121	4.969	5.283	5.526	5.536	5.459	5.692	5.051	5.835	5.835
Fe4383	1.376	2.826	3.718	4.195	4.533	4.828	5.101	5.135	5.346	5.564	5.647	5.690	5.838	5.595	6.059	6.059
Ca4455	0.761	1.107	1.294	1.395	1.481	1.546	1.623	1.604	1.670	1.746	1.761	1.732	1.800	1.715	1.856	1.856
Fe4531	1.956	2.540	2.833	3.001	3.129	3.343	3.343	3.327	3.418	3.525	3.547	3.522	3.613	3.487	3.704	3.704
Fe4668	2.016	3.171	3.869	4.212	4.513	4.733	5.006	4.911	5.171	5.415	5.475	5.288	5.477	5.340	5.652	5.652
H $\beta$	4.660	3.156	2.642	2.386	2.197	2.050	1.910	1.967	1.802	1.697	1.654	1.681	1.563	1.800	1.467	1.467
Fe5015	3.587	4.375	4.833	4.993	5.179	5.276	5.453	5.344	5.509	5.697	5.712	5.565	5.741	5.604	5.782	5.782
Mg <sub>1</sub>	0.021	0.042	0.056	0.066	0.071	0.077	0.084	0.086	0.090	0.094	0.097	0.097	0.101	0.099	0.108	0.108
Mg <sub>2</sub>	0.102	0.141	0.168	0.184	0.196	0.208	0.219	0.220	0.231	0.240	0.245	0.240	0.249	0.246	0.260	0.260
Mg <sub>b</sub>	1.696	2.229	2.654	2.858	3.053	3.268	3.374	3.345	3.644	3.656	3.705	3.621	3.696	3.687	3.848	3.848
Fe5270	1.714	2.207	2.471	2.614	2.729	2.806	2.905	2.890	2.971	3.057	3.088	3.059	3.157	3.070	3.206	3.206
Fe5335	1.454	1.935	2.187	2.325	2.426	2.504	2.600	2.593	2.671	2.746	2.773	2.745	2.817	2.763	2.887	2.887
Fe5406	0.804	1.144	1.330	1.449	1.519	1.582	1.650	1.656	1.708	1.758	1.783	1.771	1.829	1.776	1.881	1.881
Fe5709	0.658	0.809	0.882	0.936	0.962	0.985	1.006	1.008	1.016	1.031	1.037	1.039	1.061	1.025		

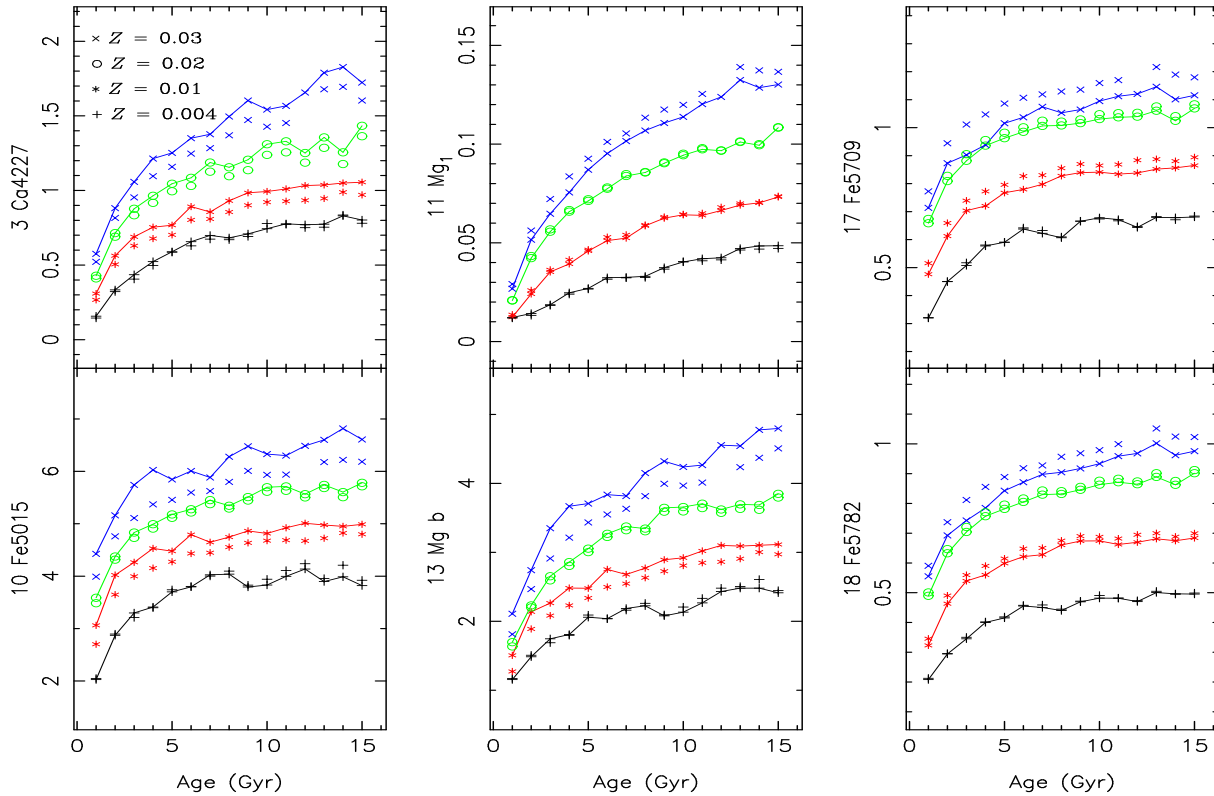


**Figure 7.** Evolution of absorption indices in the Lick/IDS system obtained by using the fitting functions for BSPs of various metallicity. The symbols linked by a line denote the indices obtained by using the high resolution spectra of González Delgado et al. (2005), and those without a line are from the low resolution spectra of Lejeune et al. (1997, 1998). Different symbols are for different metallicity, from top to bottom, the metallicity  $Z$  is 0.03, 0.02, 0.01 and 0.004, respectively.

$Z = 0.004$  to  $Z = 0.03$ . The results are presented in Table 1. We compare them with those obtained by Model A of Paper II, which uses low resolution stellar spectral library of and the fitting functions, and find that the evolution of  $\text{TiO}_1$  and  $\text{TiO}_2$  indices is not smooth for both two studies, the discrepancy in the rest 23 Lick/IDS spectral indices is small for metallicity  $Z = 0.004$  and  $Z = 0.02$ , the synthetic Ca4227 (index 3), Fe5015 (10),  $\text{Mg}_1$  (11),  $\text{Mg}_b$  (13), Fe5709 (17) and Fe5782 (18) indices show much stronger discrepancy for metallicity  $Z = 0.01$  and  $Z = 0.03$ .

In Fig. 7 we show the comparison of Ca4227 (index 3), Fe5015 (10),  $\text{Mg}_1$  (11),  $\text{Mg}_b$  (13), Fe5709 (17) and Fe5782 (18) indices between two studies. It shows that the high spectral resolution Ca4227 (3), Fe5015 (10) and  $\text{Mg}_b$  (13) indices are greater,  $\text{Mg}_1$  (11), Fe5709 (17) and Fe5782 (18) indices are less than those at low resolution for BSPs with  $Z = 0.03$  and  $Z = 0.01$ , the discrepancy is greater for BSPs with  $Z = 0.03$  in comparison to  $Z = 0.01$ . This discrepancy in the Lick/IDS spectral indices will directly influence the derived age and metallicity of a particular population, it will lower the age and metallicity if using high resolution Ca4227 (3), Fe5015 (10) and  $\text{Mg}_b$  (13) indices, and raise the age and metallicity if using high resolution  $\text{Mg}_1$  (11), Fe5709 (17) and Fe5782 (18) indices.

To discuss whether the difference of the coverage in the  $\log g - \log T_{\text{eff}}$  plane between HRES and BaSeL-2.0 libraries would cause the discrepancies in the Lick/IDS spectral absorption indices, in Figs. 8 and 9 we plot the theoretical

isochrones of the bluest (i.e., the youngest [ $\tau = 1$  Gyr] and lowest metallicity [ $Z = 0.004$ ]) and the reddest (the oldest [ $\tau = 15$  Gyr] and highest metallicity  $Z = 0.03$ ) BSPs. In order to transform the evolutionary parameters of stars along the isochrones to stellar flux for  $Z = 0.004$  BSPs in Fig. 8, we need to make interpolation in the flux grids between  $[\text{Fe}/\text{H}] = -1.0$  and  $-0.5$  because HRES spectral library only contains  $[\text{Fe}/\text{H}] = -1.0, -0.5, 0.0$  and  $0.3$ . While, the grid coverage in the  $\log g - \log T_{\text{eff}}$  plane between  $[\text{Fe}/\text{H}] = -1.0$  and  $-0.5$  is appreciably different, and the difference mainly concentrates in the low-temperature range. Within this low temperature range the denser stars (such as, low-mass MS stars) only give small contribution to the ISEDs (see Figs. 3 and 4 of Paper II), so we only interest in the difference of two libraries in the low-density range, in this range the grid coverage at  $[\text{Fe}/\text{H}] = -0.5$  is smaller than that at  $[\text{Fe}/\text{H}] = -1.0$ , so in Fig. 8 we plot the boundary of HRES flux grid coverage at  $[\text{Fe}/\text{H}] = -0.5$ . Also we plot the boundary of BaSeL-2.0 flux grid coverage at  $[\text{Fe}/\text{H}] = -0.5$ , for this library the grid coverage in the  $\log g - \log T_{\text{eff}}$  plane for  $[\text{Fe}/\text{H}] = -1.0$  and  $-0.5$  is same in the low-temperature and low-density range. Similarly, for  $Z = 0.03$  BSPs in Fig. 9, we plot the boundary of HRES flux grid coverage at  $[\text{Fe}/\text{H}] = 0.3$  and BaSeL-2.0 library at  $[\text{Fe}/\text{H}] = 0.2$ .

Comparison of the coverage in the  $\log g - \log T_{\text{eff}}$  plane for two libraries in Figs. 8 and 9 shows HRES library extends to the higher temperature, in the  $\log T_{\text{eff}} \geq 4.43$  range covers less gravity than BaSeL-2.0 library, while the latter covers

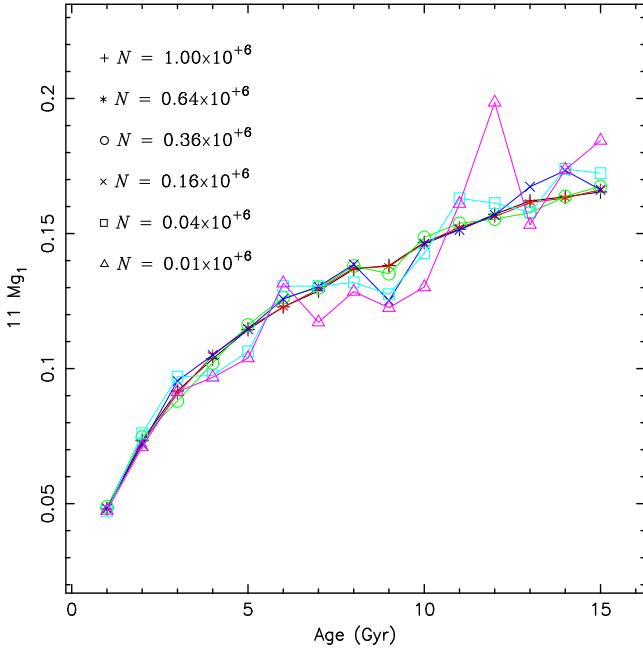


**Figure 6.** Sensibility of  $Mg_1$  index to the number of binary systems in the BSPs.

lower temperature range. Although in the high temperature range the grid coverage of two libraries exists discrepancies, both grid coverage are enough to the BSPs we considered. In the lower temperature and lower gravity range, HRES library does not cover all cool AGB stars, it would cause the discrepancies in the Lick/IDS absorption line indices. Additionally, the differences in the spectral shape caused by the resolution also would cause to the discrepancies of the above several Lick/IDS absorption line indices.

### 3.2.2 Results computed from the high-resolution spectra

To compare theoretical results with observations, the Lick/IDS absorption indices also are measured directly from the high-resolution ISEDs using the passband definitions of Worthey et al. (1994) and Worthey & Ottaviani (1997), and are presented in Table 2. In Fig. 10 we compare them (except for  $TiO_1$  and  $TiO_2$ ) with those obtained by using the fitting functions of Worthey et al. (1994) and Worthey & Ottaviani (1997) (generated from Table 1), and find that Ca4455 (index 6, almost equal for  $Z = 0.02$ ), Fe4668 (index 8, almost equal for  $Z = 0.004$ ),  $Mg_b$  (13) and Na D (19) are bluer than the corresponding ones obtained by using the fitting function for all metallicities. For Fe5709 (17) the discrepancy becomes from negative ( $Z = 0.03$ ) to positive ( $Z = 0.01$  and  $0.004$ ). Other indices are redder than the values from Table 1 for all metallicities.

Comparing the discrepancies in the Lick/IDS spectra indices caused by the difference in the metallicity, we find that the discrepancies in Ca4455 (index 6),  $Mg_2$  (12),  $Mg_b$  (13) and Na D (19) indices introduced by using the different computation method are smaller.

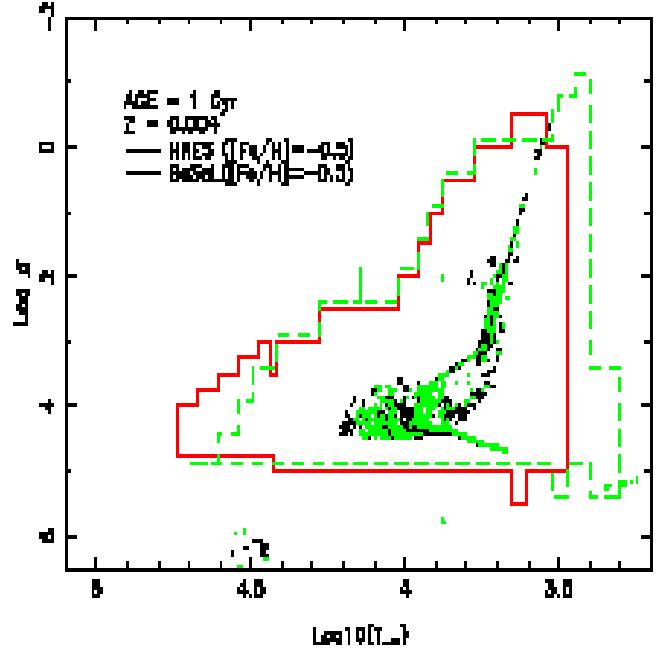


**Figure 8.** Coverage of HRES (solid line) and BaSeL-2.0 (dashed line) stellar library grids for  $[Fe/H] = -0.5$ . For the sake of clarity BaSeL-2.0 library is shifted upwards by an amount of 0.1. Over-plotted points represent the theoretical isochrone for instantaneous burst BSPs with  $Z = 0.004$  and  $\tau = 1$  Gyr. Only 200,000 binary systems are plotted and those MS stars with mass  $M \lesssim 0.7 M_{\odot}$  are removed.

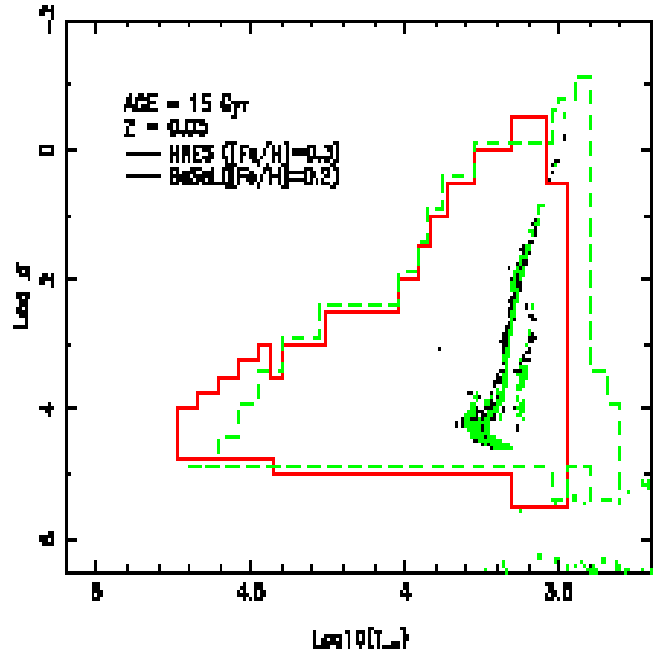


**Figure 9.** Similar to Fig. 8, but  $[Fe/H] = 0.3$  for HRES and  $[Fe/H] = 0.2$  for BaSeL-2.0 libraries,  $Z = 0.03$  and  $\tau = 15$  Gyr for the BSPs.



Table 2. Lick/IDS spectral absorption feature indices of BSPs, as measured directly from the high-resolution ISEDs (Section 3.2.2).

	Age (Gyr)														
	1.00	2.00	3.00	4.00	5.00	6.00	7.00	8.00	9.00	10.00	11.00	12.00	13.00	14.00	15.00
<i>Z</i> = 0.004															
CN <sub>1</sub>	-0.217	-0.128	-0.078	-0.052	-0.039	-0.026	-0.022	-0.017	-0.015	-0.010	-0.008	-0.011	-0.010	-0.009	-0.010
CN <sub>2</sub>	-0.166	-0.081	-0.035	-0.012	-0.001	0.010	0.013	0.016	0.019	0.022	0.024	0.022	0.023	0.024	0.022
Ca4227	0.328	0.467	0.574	0.695	0.763	0.875	0.917	0.906	0.985	1.051	1.081	1.083	1.145	1.177	1.172
G4300	-0.408	1.347	2.613	3.630	4.229	4.837	5.059	5.061	5.615	5.858	5.999	5.770	5.906	6.188	6.244
Fe4383	0.104	1.448	2.298	2.912	3.264	3.699	3.832	3.811	4.100	4.247	4.378	4.308	4.461	4.551	4.534
Ca4455	0.229	0.404	0.542	0.652	0.712	0.791	0.809	0.796	0.843	0.868	0.883	0.851	0.895	0.893	0.890
Fe4531	1.309	1.832	2.146	2.405	2.554	2.713	2.765	2.739	2.882	2.945	2.992	2.942	3.030	3.074	3.080
Fe4668	0.404	0.741	0.955	1.112	1.200	1.307	1.344	1.305	1.387	1.394	1.416	1.344	1.362	1.367	1.379
H $\beta$	6.000	4.490	3.462	2.917	2.607	2.323	2.217	2.081	2.008	1.916	1.843	1.885	1.888	1.765	1.769
Fe5015	2.413	3.420	3.983	4.429	4.631	4.911	4.974	4.882	5.113	5.203	5.236	5.125	5.275	5.290	5.303
Mg <sub>1</sub>	0.017	0.031	0.042	0.048	0.051	0.059	0.061	0.060	0.062	0.066	0.068	0.071	0.074	0.075	0.073
Mg <sub>2</sub>	0.056	0.078	0.094	0.105	0.111	0.123	0.128	0.126	0.133	0.137	0.142	0.144	0.149	0.152	0.151
Mg <sub>b</sub>	0.628	0.732	0.840	0.953	1.027	1.128	1.192	1.192	1.296	1.343	1.387	1.418	1.456	1.509	1.523
Fe5270	1.023	1.435	1.666	1.856	1.951	2.101	2.134	2.116	2.234	2.284	2.323	2.304	2.383	2.415	2.418
Fe5335	1.084	1.477	1.717	1.919	1.993	2.179	2.212	2.166	2.271	2.348	2.371	2.375	2.469	2.475	2.461
Fe5406	0.747	1.052	1.234	1.365	1.424	1.557	1.595	1.555	1.632	1.680	1.711	1.724	1.777	1.790	1.780
Fe5709	0.356	0.495	0.564	0.628	0.654	0.695	0.692	0.684	0.725	0.731	0.734	0.710	0.731	0.736	0.740
Fe5782	0.257	0.352	0.415	0.461	0.472	0.540	0.547	0.518	0.527	0.555	0.559	0.578	0.602	0.586	0.564
Na D	0.713	0.908	1.052	1.152	1.205	1.329	1.384	1.366	1.441	1.510	1.548	1.603	1.663	1.696	1.699
TiO <sub>1</sub>	0.009	0.009	0.010	0.009	0.009	0.009	0.011	0.009	0.009	0.009	0.010	0.012	0.011	0.010	0.010
TiO <sub>2</sub>	0.020	0.022	0.026	0.024	0.025	0.026	0.030	0.026	0.026	0.026	0.028	0.031	0.030	0.029	0.028
H $\delta$ A	9.757	5.890	3.371	1.853	0.997	0.131	-0.199	-0.478	-0.897	-1.266	-1.445	-1.254	-1.349	-1.657	-1.667
H $\gamma$ A	8.519	4.451	1.617	-0.240	-1.353	-2.462	-2.907	-3.168	-3.898	-4.359	-4.646	-4.384	-4.543	-5.057	-5.113
H $\delta$ F	6.969	4.834	3.271	2.334	1.797	1.283	1.094	0.874	0.663	0.441	0.346	0.491	0.458	0.253	0.245
H $\gamma$ F	6.460	4.326	2.712	1.685	1.066	0.444	0.196	-0.008	-0.355	-0.609	-0.771	-0.633	-0.678	-0.986	-1.010
<i>Z</i> = 0.01															
CN <sub>1</sub>	-0.164	-0.058	-0.027	-0.016	-0.004	0.008	0.011	0.017	0.025	0.024	0.026	0.026	0.030	0.034	0.034
CN <sub>2</sub>	-0.110	-0.011	0.016	0.026	0.037	0.047	0.049	0.056	0.064	0.063	0.064	0.065	0.068	0.072	0.072
Ca4227	0.430	0.710	0.931	1.037	1.144	1.272	1.272	1.403	1.497	1.546	1.549	1.591	1.637	1.654	1.719
G4300	0.419	2.984	4.362	4.797	5.213	5.704	5.726	6.010	6.278	6.350	6.485	6.458	6.521	6.832	6.765
Fe4383	0.997	3.022	3.963	4.364	4.760	5.182	5.235	5.592	5.843	5.930	5.993	6.071	6.190	6.336	6.410
Ca4455	0.408	0.782	0.949	1.020	1.089	1.162	1.170	1.232	1.276	1.285	1.291	1.301	1.329	1.346	1.364
Fe4531	1.953	2.742	3.086	3.222	3.363	3.502	3.510	3.645	3.737	3.784	3.805	3.821	3.883	3.942	3.979
Fe4668	0.935	1.499	1.754	1.859	1.934	2.041	2.075	2.111	2.141	2.156	2.190	2.154	2.169	2.248	2.226
H $\beta$	5.579	3.653	2.942	2.695	2.500	2.235	2.153	2.080	1.944	1.928	1.840	1.809	1.792	1.658	1.695
Fe5015	3.721	5.172	5.702	5.903	6.109	6.296	6.324	6.506	6.607	6.671	6.661	6.646	6.735	6.787	6.849
Mg <sub>1</sub>	0.030	0.056	0.069	0.075	0.083	0.090	0.090	0.099	0.104	0.107	0.107	0.109	0.113	0.113	0.118
Mg <sub>2</sub>	0.081	0.122	0.144	0.155	0.167	0.179	0.181	0.193	0.201	0.208	0.208	0.211	0.216	0.219	0.225
Mg <sub>b</sub>	0.795	1.115	1.395	1.540	1.667	1.795	1.842	1.951	2.026	2.140	2.180	2.193	2.227	2.319	2.347
Fe5270	1.513	2.095	2.377	2.501	2.636	2.753	2.792	2.912	2.984	3.034	3.053	3.080	3.132	3.182	3.216
Fe5335	1.493	2.137	2.457	2.596	2.748	2.894	2.917	3.077	3.168	3.208	3.184	3.231	3.288	3.277	3.355
Fe5406	1.079	1.552	1.774	1.880	1.992	2.096	2.116	2.231	2.294	2.349	2.332	2.347	2.396	2.403	2.467
Fe5709	0.523	0.694	0.778	0.804	0.833	0.858	0.871	0.890	0.899	0.908	0.912	0.917	0.939	0.929	0.929
Fe5782	0.342	0.536	0.639	0.679	0.733	0.778	0.769	0.832	0.862	0.864	0.825	0.840	0.861	0.817	0.865
Na D	0.937	1.336	1.556	1.673	1.811	1.915	1.951	2.086	2.168	2.262	2.254	2.284	2.348	2.380	2.462
TiO <sub>1</sub>	0.013	0.017	0.016	0.016	0.017	0.017	0.017	0.018	0.018	0.021	0.019	0.018	0.019	0.019	0.021
TiO <sub>2</sub>	0.026	0.036	0.036	0.038	0.040	0.041	0.041	0.043	0.044	0.048	0.045	0.043	0.045	0.044	0.048
H $\delta$ A	7.907	2.879	0.912	0.179	-0.603	-1.435	-1.644	-2.077	-2.639	-2.729	-2.976	-2.995	-3.181	-3.669	-3.612
H $\gamma$ A	6.638	1.004	-1.561	-2.476	-3.389	-4.410	-4.610	-5.149	-5.770	-5.948	-6.269	-6.274	-6.441	-7.108	-7.004
H $\delta$ F	6.070	3.089	1.909	1.503	1.081	0.613	0.481	0.310	-0.002	-0.030	-0.170	-0.160	-0.254	-0.537	-0.474
H $\gamma$ F	5.654	2.655	1.243	0.740	0.263	-0.315	-0.453	-0.693	-1.032	-1.122	-1.308	-1.316	-1.389	-1.755	-1.685
<i>Z</i> = 0.02															
CN <sub>1</sub>	-0.108	-0.031	-0.004	0.015	0.031	0.044	0.057	0.058	0.068	0.079	0.084	0.078	0.093	0.084	0.098
CN <sub>2</sub>	-0.053	0.016	0.041	0.059	0.074	0.087	0.100	0.099	0.110	0.122	0.127	0.122	0.136	0.126	0.143
Ca4227	0.579	1.107	1.425	1.610	1.774	1.897	2.061	2.024	2.155	2.314	2.355	2.249	2.412	2.266	2.540
G4300	1.424	4.151	5.215	5.706	6.161	6.442	6.733	6.576	6.823	7.095	7.091	6.884	7.219	6.655	7.339
Fe4383	2.107	4.127	5.158	5.765	6.278	6.658	7.107	7.054	7.420	7.835	7.966	7.813	8.252	7.870	8.550
Ca4455	0.696	1.071	1.263	1.371	1.468	1.545	1.618	1.598	1.679	1.752	1.771	1.752	1.818	1.737	1.862
Fe4531	2.612	3.370	3.728	3.913	4.083	4.209	4.352	4.316	4.464	4.608	4.641	4.611	4.730	4.574	4.867
Fe4668	1.449	1.879	2.179	2.311	2.495	2.572	2.657	2.600	2.720	2.810	2.836	2.776	2.947	2.791	2.863
H $\beta$	5.050	3.399	2.889	2.579	2.340	2.173	2.001	1.904	1.832	1.740	1.643	1.706	1.522	1.452	1.436
Fe5015	5.113	6.358	6.933	7.183	7.461	7.634	7.811	7.688	8.123	8.147	8.143	8.076	8.240	7.972	8.298
Mg <sub>1</sub>	0.048	0.076	0.094	0.106	0.116	0.123	0.133	0.134	0.142	0.150	0.155	0.151	0.161	0.159	0.170
Mg <sub>2</sub>	0.110	0.163	0.195	0.213	0.230	0.241	0.258	0.258	0.270	0.285	0.291	0.285	0.298	0.295	0.312
Mg <sub>b</sub>	0.995	1.641	2.041	2.240	2.465	2.570	2.770	2.775	2.874	3.052	3.136	3.084	3.182	3.189	3.366
Fe5270	2.043	2.601	2.921	3.115	3.269	3.382	3.511	3.514	3.623	3.741	3.797	3.807	3.816	3.831	4.024
Fe5335	2.044	2.809	3.221	3.469	3.635	3.752	3.917	3.901	3.999	4.140	4.188	4.126	4.266	4.159	4.358
Fe5406	1.433	1.966	2.273	2.431	2.579	2.667	2.809	2.787	2.894	3.016	3.060	2.991	3.109	3.068	3.194
Fe5709	0.705	0.834	0.896	0.939	0.966	0.988	1.000	1.005	1.019	1.028	1.038	1.059	1.072	1.040	1.083
Fe5782	0.495	0.803	0.955	1.040	1.084	1.118	1.172	1.150	1.186	1.222	1.221	1.157	1.214	1.167	1.215
Na D	1.250	1.809	2.142	2.334	2.499	2.602	2.772	2.793	2.909	3.045	3.115	3.080	3.209	3.208	3.364
TiO <sub>1</sub>	0.013	0.018	0.022	0.020	0.024	0.024	0.027	0.025	0.029	0.032	0.032	0.027	0.030	0.033	0.031
TiO <sub>2</sub>	0.029	0.040	0.048	0.048	0.053	0.054	0.060	0.057	0.063	0.067	0.067	0.061	0.066	0.068	0.068
H $\delta$ A	5.770	1.301	-0.464	-1.571	-2.637	-3.449	-4.261</								



#### 4 SUMMARY AND CONCLUSIONS

We have simulated realistic stellar populations composed of 100 per cent binaries by producing  $1 \times 10^6$  binary systems using a Monte Carlo technique. Using the EPS method we present the high spectral resolution (0.3 Å) ISEDs over the wavelength range 3000–7000 Å and 25 Lick/IDS spectral absorption indices, for an extensive set of instantaneous burst BSPs with binary interactions over a large range of age and metallicity:  $1 \leq \tau \leq 15$  Gyr and  $0.004 \leq Z \leq 0.03$ . This set of high spectral resolution ISEDs fully satisfies the need of studying the formation and evolution of galaxy by analyzing the data of modern spectroscopic galaxy surveys, and can be available on request.

By comparing the synthetic continuum at high and low resolution, we show that there is a good agreement for BSPs with  $Z = 0.02$  and smaller discrepancy for BSPs with non-solar metallicity. And, the comparison of the Lick/IDS spectral indices at low and high resolution, both of which are obtained by using the fitting functions, shows that the high resolution Ca4227, Fe5015 and Mg<sub>b</sub> indices are redder, Mg<sub>1</sub>, Fe5709 and Fe5782 indices are bluer than those at low resolution for BSPs with  $Z = 0.01$  and 0.03. The high spectral Ca4227, Fe5015 and Mg<sub>b</sub> indices act to lower the age and metallicity, and the high resolution Mg<sub>1</sub>, Fe5709 and Fe5782 indices will raise the age and metallicity.

At high resolution we compare the Lick/IDS spectral absorption indices obtained by using the fitting functions with those measured directly from the synthetic spectra, and find that Ca4455, Fe4668, Mg<sub>b</sub> and Na D indices are redder for all metallicities, Fe5709 is redder at  $Z = 0.03$  and becomes to be bluer at  $Z = 0.01$  and 0.004, other indices are bluer for all metallicities than the corresponding values computed from the high-resolution ISEDs.

#### ACKNOWLEDGEMENTS

We acknowledge the generous support provided by the Chinese Natural Science Foundation (Grant Nos 10303006, 10273020 & 10433030), by the Chinese Academy of Sciences (KJCX2-SW-T06) and by the 973 scheme (NKBRSG1999075406). We are deeply indebted to Dr. Lejeune for making his BaSeL-2.0 model available to us. We also thanks to the referee for suggestions that have improved the quality of this manuscript.

#### REFERENCES

- Allard F., Hauschildt P. H., Alexander D. R., Tamanai A., Schweitzer A., 2001, ApJ, 556, 357
- Bertone E., Buzzoni A., Chavez M., Rodriguez-Merino L. H., 2003a, the MPA workshop on "Stellar Populations 2003"
- Bertone E., Rodriguez-Merino L. H., Chavez M., Buzzoni A., 2003b, RMxAC, 17, 91
- Bruzual G., Charlot S., 2003, MNRAS, 344, 1000
- Castelli F., Munari U., 2001, A&A, 366, 1003
- Chavez M., Malagnini M. L., Morossi C., 1997, A&AS, 126, 267
- Eggleton P. P., Fitchett M. J., Tout C. A., 1989, ApJ, 347, 998
- Goldberg D., Mazeh T., 1994, A&A, 282, 801
- González Delgado R. M., Leitherer C., 1999, ApJS, 125, 479
- González Delgado R. M., Cerviño M., Martins L. P., Leitherer C., Hauschildt P. H., 2005, MNRAS, 357, 945
- Gray R. O., Corbally C. J., 1994, AJ, 107, 742
- Hauschildt P. H., Baron E., 1999, J. Comp. Appl. Math., 102, 41
- Hubeny I., Lanz T., Jeffery C. S., 1995, SYNSPEC - A Users Guide
- Hurley J. R., Tout C. A., Pols O. R., 2002, MNRAS, 329, 897
- Jones L. A., 1997, PhD thesis, Univ. North Carolina
- Kurucz R. L., 1993, Kurucz CD-ROM 13
- Lanz T., Hubeny I., 2003, ApJS, 146, 417
- Le Borgne J.-F., Bruzual G., Pelló R., et al. 2003, A&A, 402, 433
- Lejeune T., Cuisinier F., Buser R., 1997, A&AS, 125, 229
- Lejeune T., Cuisinier F., Buser R., 1998, A&AS, 130, 65
- Martins L., Delgado González R. M., Leitherer C., Cerviño M., Hauschildt P., 2005, MNRAS, 358, 49
- Mazeh T., Goldberg D., Duquennoy A., Mayor M., 1992, ApJ, 401, 265
- Munari U., Sordo R., Castelli F., Zwitter T., 2005, A&A, submitted (astro-ph/0502047)
- Murphy T., Meiksin A., 2004, MNRAS, 351, 1430
- Miller G. E., Scalo J. M., 1979, ApJS, 41, 513
- Prugniel P., Soubiran C., 2001, A&A, 369, 1048
- Sánchez-Blázquez P., Jimenez J., Peletier R., et al., 2003, RMxAC, 17, 192
- Tantalo R., Chiosi C., Munari U., Piován L., Sordo R., 2004, MNRAS, submitted (astro-ph/0406314)
- Vazdekis A., 1999, ApJ, 513, 224
- Worthey G., Faber S. M., Gonzalez J. J., Burstein D., 1994, ApJS, 94, 687
- Worthey G., Ottaviani D. L., 1997, ApJS, 111, 377
- Xin Y., Deng L., 2005, ApJ, 619, 824
- Zhang F., Han Z., Li L., Hurley J. R., 2004, A&A, 415, 117 (Paper I)
- Zhang F., Han Z., Li L., Hurley J. R., 2005, MNRAS, 357, 1088 (Paper II)
- Zwitter T., Castelli F., Munari U., 2002, in Munari U., ed., ASP. Conf. Ser. Vol. 298, GAIA spectroscopy, Science and Technology, Astron. Soc. Pac., San Francisco, p.215
- Zwitter T., Castelli F., Munari U., 2004, A&A, 417, 1055

This paper has been typeset from a  $\text{\TeX}$ / $\text{\LaTeX}$  file prepared by the author.